

A Remedy for Proposal Failures in Metropolis Light Transport

ANONYMOUS AUTHOR(S)

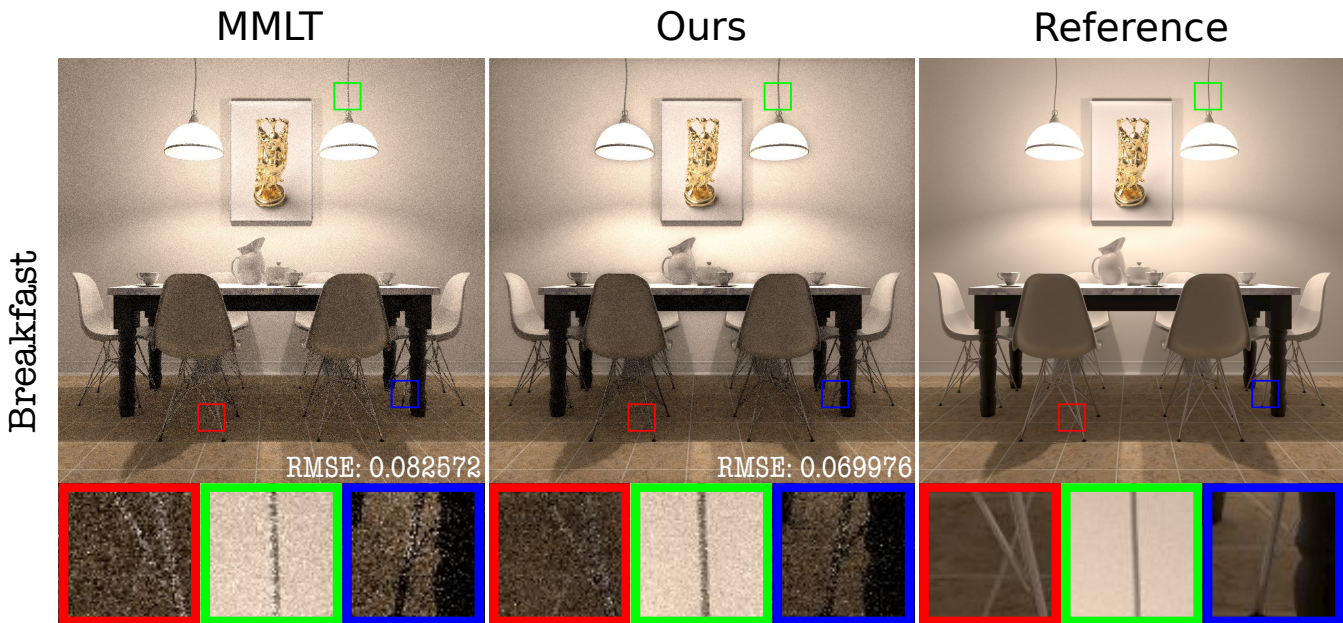


Fig. 1. *The Breakfast scene.* Equal-time comparison. Left: Image rendered with MMLT shows suboptimal performance, because more than 37% of the paths that were used to reconstruct the image carried no radiance. Middle: Giving special treatment to those zero-contribution paths, our method reduces the percentage to less than 2% and exhibits much better results with smaller RMSE. If our method is used to produce the same RMSE/quality result as MMLT does, in general, about a third of the computation will be saved.

We study MLT-type algorithms building on bidirectional path tracing. We call the failure of obtaining a complete mutation path, which may be caused by the failure of tracing required two sub-paths or the failure of connecting the two sub-paths, as *Proposal Failure*. This kind of proposal failure path could break the detailed balance condition of Markov chain, which means none Markov chain really reaches its equilibrium. Considering that proposal failure can not be avoided, all MLT-type algorithms, to some extent, are biased, and the problem becomes more serious for MMLT because the fact that it runs many independent Markov chains and every chain explores paths of a fixed depth value increases its chance of confronting proposal failure paths. To address this problem, based on MMLT, we propose a novel algorithm, Proposal Failure MLT (PFMLT), which excludes proposal failure paths from the states of Markov chain. PFMLT could be the first unbiased MLT-type algorithm. With various scenes of challenging lighting, geometry and material tested, PFMLT always produced better results than MMLT did.

CCS Concepts: • Computing methodologies → Computer graphics;

Permission to make digital or hard copies of part or all of this work for personal or classroom use is granted without fee provided that copies are not made or distributed for profit or commercial advantage and that copies bear this notice and the full citation on the first page. Copyrights for third-party components of this work must be honored. For all other uses, contact the owner/author(s).

© 2019 Copyright held by the owner/author(s).

0730-0301/2019/7-ART1 \$15.00

<https://doi.org/>

Additional Key Words and Phrases: rendering

ACM Reference format:

Anonymous Author(s). 2019. A Remedy for Proposal Failures in Metropolis Light Transport. *ACM Trans. Graph.* 1, 1, Article 1 (July 2019), 14 pages. <https://doi.org/>

1 INTRODUCTION

Physically-based rendering is extensively used now, but solving the rendering equation is still a laborious task, especially for scenes with challenging lighting, geometry or material.

[Veach 1997] introduced Metropolis-Hastings Sampling ([Hastings 1970; Metropolis et al. 1953]) into computer graphics and presented the original Metropolis Light Transport (MLT). The main advantage of MLT is that the path space is explored locally by making small mutations to the current path to generate proposal path, which makes MLT a substantially efficient rendering algorithm for particularly challenging scenes. However, MLT's mutation rules are complex and none of the rules is symmetric, which makes its implementation a significant undertaking.

[Kelemen et al. 2002] presented Primary Sample Space MLT (PSSMLT), whose mutation strategy in the unit cube of pseudo-random numbers is symmetric and easy to implement. [Hachisuka et al. 2014] presented an extension to PSSMLT named Multiplexed

117 Metropolis Light Transport (MMLT) which combines MCMC meth-
 118 ods with Multiple Importance Sampling [Veach 1997].

119 Some Adaptive mutation strategies working in path space or
 120 primary sample space have been developed, such as MEMLT [Jakob
 121 and Marschner 2012] for specular interactions, HSLT [Hanika et al.
 122 2015] for rough materials, and GeoMLT [Otsu et al. 2018], which
 123 incorporates visibility into mutation strategies of MCMC rendering,
 124 and H2MC [Li et al. 2015], which is based on MMLT’s approach and
 125 utilizes Hamiltonian Monte Carlo to adaptively control the shape
 126 of the transition kernels.

127 Also, several methods have been developed to bridge path space
 128 and primary sample space by using invertible mappings to transform
 129 samples between them, such as [Bitterli et al. 2018; Otsu et al. 2017;
 130 Pantaleoni 2017].

131 Unfortunately, the percentage of the paths that are used to re-
 132 construct image carried no radiance in all of those algorithms is
 133 still high for challenging scenes, which brings serious variance to
 134 the final image. This paper provide a simple but efficient way to re-
 135 duce the percentage substantially without any upgrades of mutation
 136 strategies.

137 We consider the proposal paths of zero-contribution as proposal
 138 failures and distinguish them from normal proposal paths. In order
 139 to improve the quality of the final image, the contribution of every
 140 valid sampled path should be approximately proportional to the
 141 probability with which it was sampled. So, when proposal failure
 142 happens, instead of repeatedly accumulating the contribution of
 143 the current path like current MLT-type algorithms do, our algo-
 144 rithm nullifies the proposal failure. The nullification involves two
 145 operations: (1)skipping the repeated accumulation of the current
 146 path; (2)switching sample counter backward so that failure paths
 147 are excluded. But, if the number of proposal failures of the current
 148 path surpasses some threshold value which can be set by users, we
 149 stop the nullification. Because, in the areas around which it is hard
 150 to find a complete path, introducing some extra noises like current
 151 MLT-type algorithms do is better than undersampled.

152 Though the nullification of some proposal failures means extra
 153 overhead must be paid for finding a valid sample path, our method
 154 substantially decreases the percentage of zero contribution paths
 155 used to reconstruct the final picture. As a result, MLT-type rendering
 156 algorithms extended with our method will be much more efficient
 157 than the original algorithms. As exemplified in Figure 1, compared
 158 to MMLT, our method reduces the percentage of zero-radiance paths
 159 that were used to reconstruct the final image from 37% to less than
 160 2%, and produces the image of higher quality. If our method is used
 161 to produce the same RMSE/quality result as MMLT does, about a
 162 third of the computation will be saved. What’s more, our method
 163 can be easily extended to all MLT-type algorithms.

164 In summary, the contributions of this paper are:

- 167 (1) Introduction of the concept of proposal failure.
- 168 (2) A novel extension of Metropolis sampling algorithm which
 169 simulates proposal failures and provides a remedy for them.
- 170 (3) Combination of the novel extension of Metropolis sampling
 171 with MMLT.

2 RELATED WORK

175 *Light Transport Simulation.* Light transport equation was first de-
 176 scribed by [Kajiya 1986]. [Veach 1997] presented that light transport
 177 simulation can be expressed as the integral:

$$I_j = \int_{\Omega} h_j(\bar{x}) f(\bar{x}) d\mu(\bar{x}) \quad (1)$$

182 , where I_j is the intensity of the j-th pixel of image, $\Omega = \bigcup_{k=1}^{\infty} \Omega_k$ is
 183 the space of light paths of all finite lengths k, \bar{x} is a light path, $h_j()$
 184 is the reconstruction filter that selects out all the light paths that
 185 contribute to the j-th pixel, f is the contribution of \bar{x} and μ is the
 186 area measure.

187 *Monte Carlo Integration.* The integral in Equation (1) is infinite-
 188 dimensional because of the length of \bar{x} can be infinite, which cannot
 189 be solved analytically. Monte Carlo numerical integration methods
 190 provide one solution to this kind of problem. The Monte Carlo
 191 integration estimator of Equation (1) is:

$$I_j \approx \hat{I}_j = \frac{1}{N} \sum_{i=1}^N \frac{h_j(\bar{x}^{(i)}) f(\bar{x}^{(i)})}{p(\bar{x}^{(i)})} \quad (2)$$

195 , where $\bar{x}^{(i)}$ is the i-th independently sampled light path, $p(\bar{x}^{(i)})$ is
 196 the probability density of the sample and N is the total number of
 197 samples.

198 In order to decrease the variance of the estimator, $p(\bar{x}^{(i)})$ should
 199 be approximately proportional to $f(\bar{x}^{(i)})$. Unfortunately, $f(\bar{x}^{(i)})$ is a
 200 spectrally valued function, and thus there is no unambiguous notion
 201 of what it means to generate samples proportional to $f(\bar{x}^{(i)})$. To
 202 address this issue, a scalar contribution function f^* is defined as
 203 the luminance of the path contribution f . Intuitively, $p(\bar{x}^{(i)})$ can be
 204 $f^*(\bar{x}^{(i)})/b$ (where b is the normalization constant $\int_{\Omega} f(\bar{x}) d\mu(\bar{x})$). So,
 205 Equation (2) can be presented as:

$$I_j \approx \hat{I}_j = \frac{b}{N} \sum_{i=1}^N \frac{h_j(\bar{x}^{(i)}) f(\bar{x}^{(i)})}{f^*(\bar{x}^{(i)})} \quad (3)$$

208 Now, we face two problems: calculating b and getting samples
 209 from $p(\bar{x}^{(i)})$ that is $f^*(\bar{x}^{(i)})/b$. The value b is typically estimated
 210 with another independent rendering algorithm such as bidirectional
 211 path tracing ([Lafortune and Willems 1993, 1996; Veach and Guibas
 212 1994]). Then, the only problem is how to do the sampling.

213 *Path-Space MLT..* The remaining problem in Equation (3) is how
 214 to get sample $\bar{x}^{(i)}$ in path space Ω with probability density $p(\bar{x}^{(i)})$
 215 proportional to its function value $f(\bar{x}^{(i)})$, which is so-called *impor-*
 216 *tance sampling*. Veach[Veach and Guibas 1997] originally introduced
 217 Metropolis-Hastings (MH) sampling ([Hastings 1970; Metropolis
 218 et al. 1953]) into computer graphics and proposed a novel rendering
 219 algorithm, Metropolis Light Transport (MLT).

220 The mathematical foundation of MH sampling is building a Markov
 221 Chain whose stationary distribution is exactly the target distribution.
 222 After reaching its stationary distribution, every subsequent
 223 mutation state of the Markov Chain is a valid sample of the target
 224 distribution. However, it’s never easy to know when the stationary
 225 is reached. MH sampling provides a practically way to solve this
 226 problem. It generates a set of samples from a non-negative function
 227 f that is distributed proportionally to f’s value without waiting for
 228 f to reach its stationary distribution.

the stationary and without requiring the evaluation of b in two steps:

- *Proposal.* A new proposal path \bar{y} is obtained from current path \bar{x} by a mutation kernel $Q(\bar{y}|\bar{x})$.
- *Acceptance-Rejection.* Acceptance rate α is calculated:

$$\alpha(\bar{y}|\bar{x}) = \min\{1, \frac{f^*(\bar{y})Q(\bar{x}|\bar{y})}{f^*(\bar{x})Q(\bar{y}|\bar{x})}\} \quad (4)$$

. Then accept the proposal path \bar{y} with the probability α , otherwise reject it.

Mutation kernel Q is the key factor increasing acceptance rate and computation efficiency. In rendering algorithms, mutation kernel Q actually is the strategy to get proposal paths. The original MLT designs three mutation strategies targeting specific families of light paths, such as caustics or paths containing sequences of specular-diffuse-specular interactions. Some other mutation strategies have been developed in variants of path-space MLT, such as MEMLT [Jakob and Marschner 2012] for specular interactions, HSLT [Hanika et al. 2015] for rough materials, and GeoMLT [Otsu et al. 2018], which incorporates visibility into mutation strategies of MCMC rendering.

Primary Sample Space MLT. Mutating in path space is not symmetric, which means that $Q(\bar{x}|\bar{y}) \neq Q(\bar{y}|\bar{x})$. This makes implementing these rendering algorithms a significant undertaking and makes debugging a notorious task. [Kelemen et al. 2002] presented a new MLT-type algorithm, Primary Sample Space MLT (PSSMLT), whose mutation strategy works in the unit cube of pseudo-random numbers, which is symmetric and easy to implement. The unit cube is called Primary Sample Space U .

PSSMLT converts random numbers \bar{u} into light path \bar{x} by path sampling. \bar{x} can be thought of as being mapped from \bar{u} by the inverse cumulative distribution function $P^{-1}(\bar{u})$, where $P(\bar{u}) = \int_0^{\bar{u}} p(\bar{u}')d\bar{u}'$. That is: $\bar{x} = P^{-1}(\bar{u})$. For the brevity of notation, we define:

$$\begin{aligned} C(\bar{x}) &= \frac{f(\bar{x})}{p(\bar{x})} \\ \hat{C}(\bar{u}) &= C(P^{-1}(\bar{u})) = C(\bar{x}) \\ \hat{p}(\bar{u}) &= p(P^{-1}(\bar{u})) = p(\bar{x}) \\ \hat{h}_j(\bar{u}) &= h_j(P^{-1}(\bar{u})) = h_j(\bar{x}) \end{aligned}$$

Then, in primary sample space, Equation (1) can be expressed as:

$$I_j = \int_U \hat{h}_j(\bar{u}) \hat{C}(\bar{u}) d\bar{u} \quad (5)$$

Like Equation (3), the Monte Carlo integration estimator of Equation (5) can be presented as:

$$I_j \approx \hat{I}_j = \frac{b}{N} \sum_{i=1}^N \frac{\hat{h}_j(\bar{u}^{(i)}) \hat{C}(\bar{u}^{(i)})}{\hat{C}^*(\bar{u}^{(i)})} \quad (6)$$

, where \hat{C}^* is the luminance of the importance function \hat{C} . Mutating in primary sample space is symmetric. That is $Q(\bar{u}|\bar{v}) = Q(\bar{v}|\bar{u})$, which makes implementing PSSMLT much easier, and which also avoids the computation of the transition probabilities altogether. So,

the calculation of acceptance rate can be simplified as:

$$\alpha(\bar{v}|\bar{u}) = \min\{1, \frac{\hat{C}^*(\bar{v})}{\hat{C}^*(\bar{u})}\} \quad (7)$$

, where \bar{v} is the proposal state of \bar{u} in primary sample space.

PSSMLT makes the integrand much flatter, and increases the average acceptance rate and therefore reduces the variance. The generality of PSSMLT has led to a lot of applications, such as [Gruson et al. 2017; Hachisuka and Jensen 2011; Hoberock and Hart 2010; Kitaoka et al. 2009; Šík et al. 2016]. As mentioned before, the method of conversion from random numbers \bar{u} into light path \bar{x} is path sampling. Actually, PSSMLT adopts bidirectional path tracing to do the path sampling. Bidirectional path tracing produces many paths from a single primary sample by using different connection strategies to connect camera sub-path and light sub-path. And then, the connected path of maximum luminance is selected as the final proposal light path. Unfortunately, the process of finding the path of maximum luminance is not efficient.

Multiplexed MLT. In order to solve the efficient problem of PSSMLT, [Hachisuka et al. 2014] presented an extension to PSSMLT called Multiplexed Metropolis Light Transport (MMLT) which combines MCMC algorithm with Multiple Importance Sampling [Veach 1997]. Instead of always implementing all BDPT connection strategies and finding the path of maximum luminance, the algorithm chooses a single strategy according to an extra random number and returns its contribution scaled by the inverse discrete probability of the choice. The additional random number used for strategy selection can be mutated in the same way as the other components of \bar{u} in primary sample space. The Monte Carlo Integration estimator is generalized as:

$$I_j \approx \hat{I}_j = \sum_{i=1}^M \frac{b}{N_t} \sum_{i=1}^{N_t} \frac{\hat{h}_j(\bar{u}^{(i,t)}) \hat{w}_t(\bar{u}^{(i,t)}) \hat{C}(\bar{u}^{(i,t)})}{\hat{C}^*(\bar{u}^{(i,t)})} \quad (8)$$

, where, t is determined by the extra state dimension and is used to choose sample technique, and \hat{w}_t is a weighting function for any given path. The extension of the extra state dimension for choosing sample technique results that every mutation may change both random numbers from \bar{u} to \bar{v} and sample technique from t to t' . So, based on Equation (7), the calculation of acceptance rate is generalized:

$$\alpha((\bar{v}, t')|(\bar{u}, t)) = \min\{1, \frac{\hat{w}_{t'}(\bar{v}) \hat{C}_{t'}^*(\bar{v})}{\hat{w}_t(\bar{u}) \hat{C}_t^*(\bar{u})}\} \quad (9)$$

This generalization produces the practical effect that the Metropolis sampler mainly focus on more effective strategies that leads to greater MIS-weighted contributions to the final image. Furthermore, the individual iterations of every Markov Chain are much more efficient since they only execute a single connection strategy. Based on MMLT's approach, some developments have been made, such as H2MC[Li et al. 2015], which utilizes Hamiltonian Monte Carlo to adaptively control the shape of the transition kernels.

Bridging Path-Space and Primary-Sample-Space. In order to combine the flexibility of mutation strategies of path space MLT with the simplicity and efficiency of primary sample space MLT, several

349 methods have been developed to bridge the two state spaces by using
 350 invertible mappings to transform samples between them, such as [Bitterli et al. 2018; Otsu et al. 2017; Pantaleoni 2017].
 351

353 *Analysis and Problem Statement.* Generally, the improvements in
 354 MLT-type rendering algorithms can be classified into three categories.
 355 First, developments of mutation strategies in path space, such as
 356 MEMLT [Jakob and Marschner 2012] for specular interactions,
 357 HSLT [Hanioka et al. 2015] for rough materials, and GeoMLT [Otsu
 358 et al. 2018], which incorporates visibility into mutation strategies.
 359 Second, developments of mutation strategies in primary sample
 360 space, such as MMLT and H2MC [Li et al. 2015]. Third, bridging
 361 the two spaces, so that the developments of mutation strategies in
 362 both spaces can be used in the same algorithm framework, such as
 363 [Bitterli et al. 2018; Otsu et al. 2017; Pantaleoni 2017].
 364

365 All of these efforts are put on variant mutation strategies to
 366 increase the acceptance rate and to reduce the variance of their
 367 different aim scene scenarios. However, none of them can generally
 368 avoid the serious impact caused by the high ratio of proposal failures.
 369 For example, when MMLT is used to render *Villa Scene* in Figure 3,
 370 the ratio of proposal failures is up to 62.82%, which causes serious
 371 noise in the final image.

372 To our knowledge, all MLT-type algorithms don't distinguish
 373 these proposal failures from normal proposal light paths. Considering
 374 that the acceptance rate is zero, the contribution of the current
 375 path is accumulated again. However, in the proposal failure case,
 376 neither the contribution of the current path nor the contribution
 377 of the proposal failure path is proportional to the probability with
 378 which the proposal failure path was sampled, so the variance of
 379 Equation (2) is surely increased. Since proposal failures are un-
 380 avoidable even for the rendering algorithms with state-of-the-art
 381 mutation strategies, a natural idea comes to mind: can we find a
 382 way to minimize the impact of proposal failures? Yes, we can. Our
 383 method present a simple but robust remedy for proposal failures
 384 without any change in mutation strategies. Instead of trying to de-
 385 crease proposal failures in mutation strategy end, we take three
 386 steps to minimize the impact of proposal failures: (1), discard the
 387 proposal failure directly without accumulating any contribution; (2),
 388 eliminate the influence of the proposal failure on future proposals;
 389 (3), try a new proposal path.

3 OVERVIEW

390 The main idea of our method is distinguishing proposal failures from
 391 normal proposal paths and providing a simple remedy for proposal
 392 failures, so that minimizing the overall impact of proposal failures.
 393

394 First (Section 4), we verify the idea in math and present a novel
 395 MCMC, Proposal Failure MCMC (PFMCMC), which simulates pro-
 396 posal failures by setting function value $f(X_t)$ to 0 with failure prob-
 397 ability p_f and provides a special remedy for proposal failures. In
 398 the remedy, *MaxRep* indicates the maximum number of repetition
 399 to avoid a proposal failure and "MaxRep = 0" means no special
 400 treatment for proposal failures. In the example based on normal
 401 distribution function, we can assign different value to p_f to simulate
 402 scenes with different ratio of proposal failure and to compare the
 403 results sampled with or without the remedy available.

407 Second (Section 5), we combine PFMCMC with MMLT and present
 408 a novel light transport algorithm, Proposal Failure Metropolis Light
 409 Transport (PFMLT). In order to exhibit the advantages of PFMLT
 410 over MMLT, we test several different scenes with challenging light-
 411 ing, geometry and material. PFMLT always produces much better
 412 results than MMLT does in the tests, as shown in Figure 1 and
 413 Figure 3.

4 METHOD

415 An adaptive MCMC algorithm would automatically tune the param-
 416 eters of its proposal distribution, [Brooks et al. 2011; Shaby and Wells
 417 2010]. Some adaptive MCMC algorithms have been developed for
 418 various problems in different fields, such as [Giordani and Kohn 2006;
 419 Haario et al. 2001; Roberts and Rosenthal 2009; Vihola 2012]. Unfor-
 420 tunately, all of these adaptive algorithms are either too complicate or
 421 too inefficient for rendering. Furthermore, all of them consider that
 422 drawing proposal value from current state of Markov chain never
 423 fails, which is not true for MLT-type rendering algorithms. For ex-
 424 ample, Multiplexed Metropolis Light Transport (MMLT) [Hachisuka
 425 et al. 2014] has trouble searching light-carrying paths in Breakfast
 426 scene (As exemplified in Figure 1): about 37 percent of the generated
 427 paths don't carry any radiance. These zero-radiance paths corre-
 428 spond to the failures of proposal. Without mechanism of failure
 429 handling, the state-of-the-art MLT-type algorithms still just reject
 430 the proposal failures. Rejection is equivalent to generating a sample
 431 in the same place as current state, so this kind of rejections result
 432 extra noises in the final image.

433 Here, we come up with a simple but efficient adaptive MCMC
 434 algorithm specially for light transport model. We call it Proposal
 435 Failure MCMC (PFMCMC), which simulates proposal failures by
 436 setting function value $f(X_t)$ to 0 with failure probability p_f and
 437 provides a special remedy for proposal failures.

4.1 Math

440 Our algorithm, PFMCMC, restricts focus to the case of proposal fail-
 441 ure. PFMCMC is an extension of Metropolis Hastings (MH) [Hast-
 442 ings 1970; Metropolis et al. 1953], one of the most popular, classical
 443 MCMC algorithms. PFMCMC proceeds according to Algorithm 1.
 444 We aggregate some important terms of our notation in Table 1 for
 445 reference.

446 From Algorithm 1, we can see that the basic structure of PFM-
 447 CMC is similar to MH's. The major modification is that PFMCMC
 448 introduces probability p_f to simulate proposal failure, which is
 449 corresponding to the red part (line 5 to 8) in the pseudocode of
 450 Algorithm 1, and provides a remedy for the failure situation in the
 451 blue part (line 9 to 14).

452 *Proposal Failure Simulation.* $f(X_t)$ is the function of sample X_t
 453 (we think of samples with function values being zero as proposal fail-
 454 ures). p_f indicates the overall probability of proposal's random fail-
 455 ure. Generally, the percentage of zero-contribution paths in MMLT
 456 for our test scenes, like Breakfast scene in Figure 1, is between
 457 35% and 65%. So, usually, reasonably, users can set p_f at a value in
 458 $[0.35, 0.65]$ to verify the effectiveness of PFMCMC.

459 *Proposal Failure Remedy.* The basic idea of the remedy for pro-
 460 posal failure is discarding the current failure proposal and proposing

Table 1. Table of notation

Symbol	Explanation
X	Sample result set
X_0	Initial sample
X^*	Proposal sample
X_t	Current sample
X_{t+1}	Next sample
$f(X^*)$	Function value of proposal sample
$f(X_t)$	Function value of current sample
$sTotalNum$	Set number of total proposal
$rTotalNum$	Real number of total proposal
$TotalRep$	Total number of repetition for proposal failure
j	Proposal counter
p_f	Probability of proposal failure
$MaxRep$	Maximum number of repetition
CNT	Repetition counter
α	Acceptance rate

Require: Set initial values X_0 , $sTotalNum$, failure possibility p_f and the maximum number of repeating $MaxRep$.

Ensure: output sample set X

```

1:  $CNT \leftarrow 0$ 
2: for  $j = 0$  to  $sTotalNum$  do
3:   Draw a proposal value  $X^*$  from  $X_t$ 
4:   Calculate  $f(X^*)$ 
5:   Draw  $v \sim U(0, 1)$ .
6:   if  $v < p_f$  then
7:      $f(X^*) \leftarrow 0$ 
8:   end if
9:   if ( $f(X^*) == 0$ ) and ( $CNT < MaxRep$ ) then
10:     $j --$ 
11:     $CNT ++$ 
12:    continue
13:   end if
14:    $CNT \leftarrow 0$ 
15:   Calculate acceptance rate  $\alpha$ .  $\alpha = \min \{1, \frac{f(X^*)}{f(X_t)}\}$ 
16:   Draw  $u \sim U(0, 1)$ .
17:   if  $u < \alpha$  then
18:      $X_{t+1} \leftarrow X^*$ 
19:   else
20:      $X_{t+1} \leftarrow X_t$ 
21:   end if
22: end for
23: return  $X$ 

```

Algorithm 1. *Proposal Failure MCMC (PFMCMC)*. This is an extension of MH sampling, which simulates proposal failures by setting function value $f(X_t)$ to 0 with failure probability p_f (as shown in the red part) and gives a special remedy to proposal failures (as shown in blue part).

again expecting a success within the maximum times of repetition $MaxRep$. If the current proposal X^* fails, we discard it and start a new proposal all over again. If we have tried $MaxRep$ times before getting a success, we don't try any more and move forward. In the process, CNT acts as the counter of repetition. This mechanism of proposal repetition which increases the total number of proposal seems to be inefficient, but it turns out to be more efficient because of the fact that it substantially decreases the ratio of zero-function-value samples. So, this remedy ensures that the overall distribution of samples is much more approximately proportional to the contribution that the samples make to the target probability distribution function.

Note that discarding proposal failures includes two major operations. First, do not accumulate the contribution of the current path. Second, shift j backward (as " $j - -$ " in Algorithm 1), so that undo all modifications caused by the current proposal failures. The second operation is very important when j is used in the process of drawing a proposal value X^* from X_t , because this operation actually prevents next proposal value X^* from the impact of the current proposal failure.

4.2 Example

In order to illustrate the effect of PFMCMC, we'll show how it can be used to sample a 1D model based on a normal distribution function with a probability p_f of proposal failure. The effect comparison of PFMCMC and MCMC is based on equal sampling time. Considering different systems, such Mac, Windows and Linux, have different performance, we use the total number of proposal $rTotalNum$ as an indicator of sampling overhead, which is more reliable because of the elimination of influences of system performance. For MCMC, $rTotalNum$ equals to $sTotalNum$. For PFMCMC, $rTotalNum$ is the additive result of $sTotalNum$ and $TotalRep$ which is related to p_f and $MaxRep$.

Parameter Setting. We are assuming that, for the normal distribution function, the mean is 3 and the standard deviation is 2. Considering that the percentage of proposal failure for most of scenes rendered with MMLT locates in the interval [0.4, 0.6], we test two cases with p_f set at 0.4 and 0.6 respectively. $MaxRep$ is fixed at 4. For MCMC, $sTotalNum$ is set at 1600. For PFMCMC, in order to make $rTotalNum$ close at 1600, $sTotalNum$ setting is more complicate, which is affected by p_f : when p_f is 0.4, we set $sTotalNum$ at 960; when p_f is 0.6, we set $sTotalNum$ at 690.

Results Analysis. Figure 2 demonstrates the sample results of MCMC and PFMCMC. (a) and (d) show reference sample results sampled with MCMC in the condition of zero- p_f , which is the case of normal MH sampling; (b) and (e) show the results sampled with the extension of MCMC, which includes failure simulation and no remedy; (c) and (f) show the results sampled with the extension of MCMC, which is our PFMCMC including both failure simulation and remedy. From (b) and (c), we can see that PFMCMC gets better results than MCMC does when p_f being set to 0.4. From (e) and (f), we can see that PFMCMC also gets better results than MCMC does when p_f being set to 0.6.

Because of the use of correlated samples, a single run of an MCMC integrator may not be representative. We test every case

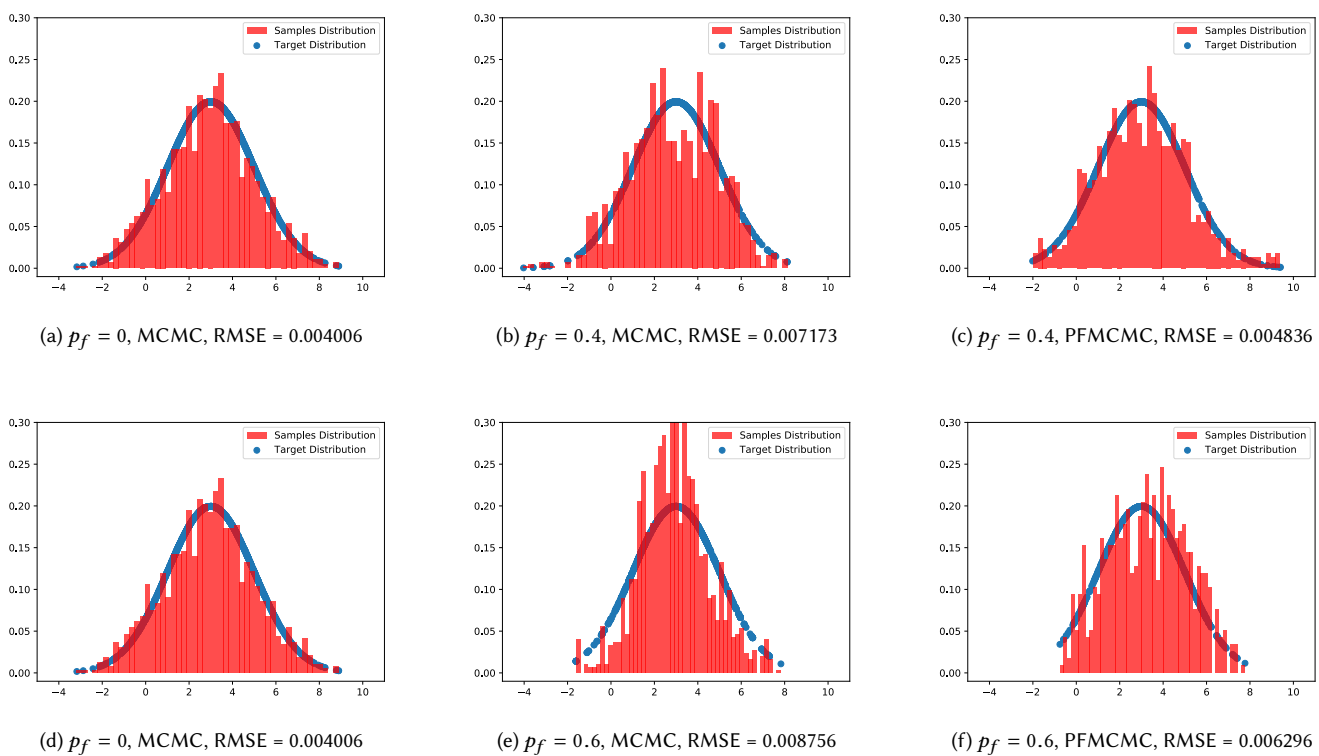


Fig. 2. PFMCMC is used to sample 1D normal distribution model with proposal failure probability p_f . The total number of proposal is used as an indicator of sampling overhead. All of these results are produced with equal number of total proposal, 1600. (a) and (d) show reference sample results sampled with MCMC in the condition of zero- p_f , which is the case of normal MH sampling; (b) and (e) show the results sampled with the extension of MCMC, which includes failure simulation and no remedy; (c) and (f) show the results sampled with the extension of MCMC, which is our PFMCMC including both failure simulation and remedy. From (b) and (c), we can see that PFMCMC gets better results than MCMC does when p_f being set to 0.4. From (e) and (f), we can see that PFMCMC also gets better results than MCMC does when p_f being set to 0.6.

Table 2. Table of average result of 100 times

Reference $(p_f==0, \text{MCMC})$	$rTotalNum: 1600$	RMS: 0.004983
	$p_f==0.4$	$p_f==0.6$
MCMC	$rTotalNum: 1600$	$rTotalNum: 1600$
	RMSE: 0.006834	RMSE: 0.008760
PFMCMC, (similar rTotalNum)	$rTotalNum: 1584$	$rTotalNum: 1589$
	RMSE: 0.006370	RMSE: 0.007728
PFMCMC, (similar RMSE)	$rTotalNum: 1383$	$rTotalNum: 1262$
	RMSE: 0.006787	RMSE: 0.008686

for 100 times and average the corresponding results, which are recorded in Table 2. Row "PFMCMC, (similar $rTotalNum$)" of the table shows that PFMCMC produces higher quality results than MCMC with similar overhead ($rTotalNum$), which supports the results shown in Figure 2 well. Less RMSE means higher quality. But, RMSE numbers may not be intuitive enough. In order

to fully exhibit the superiority of PFMCMC, we tune its parameters so that it produces similar quality results to MCMC, which is shown in Row "PFMCMC, (similar RMSE)" of the table. We can see that PFMCMC pays much less overheads to achieve results similar to MCMC's. For example, in the case " $p_f==0.4$ ", PFMCMC only pays $1383/1600 (\approx 0.8643)$ of MCMC's overheads, and in the case " $p_f==0.6$ ", the ratio is $1262/1600 (\approx 0.7888)$.

5 IMPLEMENTATION

Although we can integrate PFMCMC framework with any current MLT-type algorithms with mutation in primary sample space or path space, in this section, we will describe our rendering algorithm, Proposal Failure Metropolis Light Transport (PFMLT), by recasting MMLT ([Hachisuka et al. 2014]) in the framework of PFMCMC. MMLT improves rendering efficiency by selecting seed path with probability proportion to its contribution to the final image. Fusing MMLT with the idea of proposal failure remedy of PFMCMC makes PFMLT even much more efficient than MMLT. For example, rendering Breakfast scene (As exemplified in Figure 1) with PFMLT

```

697 Require: The maximum number of repeating MaxRep.  

698 Ensure: Accumulation of Path Contributions  

699 1: Sample a seed path  $\bar{s}$  from Initial Path Set  

700 2: Calculate the depth of  $\bar{s}$ ,  $k$  and path contribution  $f(\bar{x}_s)$   

701 3:  $\bar{s}$  is used as current path  $\bar{x}$ :  $\bar{x} \leftarrow \bar{s}$ ,  $f(\bar{x}) \leftarrow f(\bar{x}_s)$   

702 4: CNT  $\leftarrow 0$   

703 5: IsFailure  $\leftarrow 0$   

704 6: if MaxRep is not given then  

705 7:   MaxRep  $\leftarrow (k + 2)$   

706 8: else  

707 9:   MaxRep  $\leftarrow \min\{\text{MaxRep}, k + 2\}$   

708 10: end if  

709 11: for  $j = 0$  to sTotalNum do  

710 12:   Draw a proposal vector of random numbers  $\bar{v}$  from  $\bar{u}$ .  

711 13:    $t \leftarrow \text{int}((k + 2)v_s)$   

712 14:    $s \leftarrow (k + 1) - t$   

713 15:   if  $!(\bar{y}_{camera} \leftarrow \text{SampleCameraSubpath}(\bar{v}_{camera}, t))$  then  

714 16:     IsFailure  $\leftarrow 1$   

715 17:   end if  

716 18:   if  $!(\bar{y}_{light} \leftarrow \text{SampleLightSubpath}(\bar{v}_{light}, s))$  then  

717 19:     IsFailure  $\leftarrow 1$   

718 20:   end if  

719 21:   end if  

720 22:   if  $!(\bar{y}_{connect} \leftarrow \text{Connect}(\bar{y}_{camera}, \bar{y}_{light}, \bar{v}_{connect}))$  then  

721 23:     IsFailure  $\leftarrow 1$   

722 24:   end if  

723 25:   end if  

724 26:   if  $(\bar{y}_{failure})$  and (CNT < MaxRep) then  

725 27:      $j \leftarrow -$   

726 28:     REJECT()  

727 29:     CNT  $\leftarrow 0$   

728 30:     IsFailure  $\leftarrow 0$   

729 31:     Continue  

730 32:   end if  

731 33:   if  $!(\bar{y}_{failure})$  then  

732 34:     Calculate acceptance rate  $\alpha$ .  $\alpha = \min\{1, \frac{L(f(\bar{y}))}{L(f(\bar{x}))}\}$   

733 35:      $u \sim U(0, 1)$ .  

734 36:     if  $u < \alpha$  then  

735 37:        $\bar{x} \leftarrow \bar{y}$   

736 38:       ACCEPT()  

737 39:     else  

738 40:       REJECT()  

739 41:     end if  

740 42:     AccumulatePathContribution( $f(\bar{x})$ ,  $f(\bar{y})$ )  

741 43:   end for

```

Algorithm 2. *PFMLT* (*Proposal Failure MLT*). The blue part is the simple remedy for proposal failures. When proposal failure is detected, we'll try at most *MaxRep* times to avoid it, so that to minimize its impact on the final image.

saves about 30 percent of time to produce the same quality image as MMLT does. Algorithm 2 shows the pseudocode of PFMLT.

Initialization. First, the same as MMLT, we sample a seed path \bar{s} from Initial Path Set and calculate its depth k and contribution $f(\bar{x}_s)$. The depth k should be emphasized here, like MMLT, all of subsequent proposal paths are of the same depth as this seed path. Seed path \bar{s} should be assigned to current path \bar{x} . *sTotalNum* can be obtained by dividing total proposal number by total number of Markov chains. Then, some special variables for implementing the core idea of PFMCMC should be initiated. Both proposal failure flag *IsFailure* and repeating counter *CNT* are initiated as 0. As to the maximum number of repeating *MaxRep*, if its value is not given by users, we set it at $k + 2$, which is an experiment value that makes PFMLT perform well enough. If users provide a value for *MaxRep*, the smaller value in the user-value and $k + 2$ will be used as the final *MaxRep*. This mechanism enables users to effectively adjust *MaxRep* for some extremely challenging scene to produce better results.

Random Numbers Proposal. For MMLT, the same as PSSMLT, two main steps are needed to draw a proposal \bar{y} from \bar{x} in path space. Firstly, draw a proposal vector of random numbers \bar{v} from \bar{u} which is the primary sample space counterpart of \bar{x} . Secondly, obtain \bar{y} by path sampling in path space using the proposal vector of random numbers \bar{v} . As to the first step, note that we apply normally distributed perturbations to each component of the vector of random numbers. The advantage of sampling with a normal distribution like this is that it naturally tries a variety of mutation sizes. It preferentially makes small mutations that remain close to the current state, which help locally explore the path space in small areas of high contribution.

Path Sampling and Potential Failures. As mentioned in "Random Numbers Proposal" part, the second step of path proposal is path sampling. It is this step where proposal failures occur. The proposal vector of random numbers \bar{v} has four main uses in path sampling. First, one random number, v_s , of \bar{v} is used to choose sample technique, so that t and s are determined. Second, a sub-vector, \bar{v}_{camera} , of \bar{v} , along with t , is used to sample a camera sub-path \bar{y}_{camera} with depth exactly being t . Third, a sub-vector, \bar{v}_{light} , of \bar{v} , along with s , is used to sample a light sub-path \bar{y}_{light} with depth exactly being s . Fourth, a sub-vector, $\bar{v}_{connect}$, of \bar{v} is used to connect \bar{y}_{camera} and \bar{y}_{light} to make a complete proposal path \bar{y} and to calculate proposal path contribution $f(\bar{y})$.

Except for the first stage, the other three are of potential failures. In the sampling sub-path stages, the depth of camera sub-path \bar{y}_{camera} may not be t , or the depth of light sub-path \bar{y}_{light} may not be s , so failures happen. In the connecting stage, the connection between the two sub-paths, \bar{y}_{camera} and \bar{y}_{light} , may be blocked, which is a very high probability event. The existence of these failures is the very reason why PFMLT is much more efficient than MMLT.

Failure Remedy. *IsFailure* is used to indicate whether any failure has happened. If any failure is detected, the flag *IsFailure* is set to 1. Note that if a failure has been detected earlier, the latter path sampling programs are not necessary to run.

MMLT, which does not give any special care to proposal path failures, just rejects the failure proposal path and accumulates the contribution of the current path. However, neither the contribution of the current path nor the contribution of the proposal failure path is proportional to the probability with which the proposal failure path was sampled, which surely introduces a lot of extra noises.

Our method, PFMLT, will reduce this kind of noise substantially. If failure happens in the process of obtaining proposal path \bar{y} , we don't even get into the step of calculating acceptance, not to mention repeatedly accumulating the contribution of the current path. We just discard the whole current proposal, including the trace of the proposal vector of random numbers \bar{v} , and try a new proposal base on the current path, which is shown in Line 28 to Line 34 of Algorithm 2. The maximum number of this kind repeating is $MaxRep$. If we have try $MaxRep$ path proposals of some current path, we don't try any more and just move forward like MMLT does, because we find that too many repetitions will decrease overall efficiency. As mentioned in Initialization part, the default value of $MaxRep$ is set at $k + 2$, and users can tune the value to reach an even higher efficiency for some extremely challenging scene. When we move forward, both proposal failure flag *IsFailure* and repeating counter *CNT* should be reset.

Again, note that Line 29 in Algorithm 2, " $j--$ ", is very important. Because j is used to draw proposal vector of random numbers \bar{v} from \bar{u} in primary sample space. " $j--$ " is the very operation that prevents the new proposal " \bar{v} " from the impact of the current proposal failure. We show the related test images in Appendix A.

Accept Probability. Considering that e used the same mutation function for getting the vector of random numbers \bar{v} from \bar{u} as MMLT. Since these mutations are all symmetric, transition probability density functions are not needed to evaluate. The acceptance probability α is simply the ratio of the luminosities of proposal path contribution $f(\bar{y})$ and current path contribution $f(\bar{x})$.

Contribution Accumulation. The same as MMLT, the scaling by the reciprocal of the discrete probability density of the selected path length as noted before, we also need to scale each contribution by the number of techniques $k + 2$. This scaling corresponds to the fact that the chain explores $k + 2$ different sub-spaces.

6 RESULTS

This section includes two subsections, "Main Results" and "Extra Results". In the "Main Results", we implement our method by extending the system of PBRT, and we compare against MMLT implemented in the same system. In the "Extra Result", we show that our method can be easily used to extend other systems and extend both RJMLT and MMLT in Tungsten [Bitterli 2017], a renderer that is a much simpler and faster than PBRT, and we compare against MMLT and RJMLT implemented in Tungsten.

6.1 Main Results

We implement our method by extending the system of PBRT, and we compare against MMLT implemented in the same system. Five scenes – Breakfast (1024×1024), Villa (1200×580), Bathroom (1280×720), Bidir (768×576), Living Room (1280×720) – with different geometry, lighting and material configurations are rendered using

Mac pro with Intel Core i5 at 2.7GHz. Villa scene reference is rendered using MMLT in PBRT and the references of the other four scenes are rendered with BDPT in PBRT. Rendering each of those references costs several days of computation. We set the maximum path length at 9 for Living Room scene and at 5 for the other four scenes. The value of *MaxRep* is set at $k + 2$ by default.

Equal-time Comparison. We show the image comparison results in Figure 1 and Figure 3. To make equal-time comparisons between MMLT and our method, we rendered all the five scenes. Because of extra overheads for failure remedy in our method, the parameter of mutations per pixel should be set at a smaller value than in MMLT, as show Column "Mutations Per Pixel" of Table 3.

In order to obtain the statistic data of these comparisons, we define some counters in Algorithm 2: *TotalPaths* is the total number of paths traced; *RemedyPaths* is the number of paths traced for the remedy of proposal failures, which is the extra overhead of our method; *FinalFailurePaths* is the number of final failure paths after remedy; *AcceptancePaths* is the number of paths accepted. All of these counters should be initialized to 0 before the beginning of rendering (Line 11 of Algorithm 2). In the Algorithm 2, we add some other code for statistics: "*TotalPaths* +="; at Line 12; "*RemedyPaths* +="; at Line 29; "*if*($\alpha < 0.00001$)*FinalFailurePaths* +="; at Line 37; "*AcceptancePaths* +="; at Line 40. We use the following equations to calculate *FailureRate* and *AcceptanceRate*.

$$\text{FailureRate} = \frac{\text{FinalFailurePaths}}{(\text{TotalPaths} - \text{RemedyPaths})}$$

$$\text{AcceptanceRate} = \frac{\text{AcceptancePaths}}{(\text{TotalPaths} - \text{RemedyPaths})}$$

These statistics are also recorded in Table 3.

Scenes	Algorithms	Mutations Per Pixel	Failure Rate	Acceptance Rate	RMSE
Breakfast	MMLT	150	37.37%	49.38%	0.082572
	Ours	100	1.54%	77.84%	0.069976
Villa	MMLT	200	62.82%	32.39%	0.083772
	Ours	80	10.47%	75.26%	0.070404
Bathroom	MMLT	280	40.00%	57.00%	0.120891
	Ours	150	5.88%	89.01%	0.103564
Bidir	MMLT	75	37.40%	57.82%	0.067776
	Ours	45	1.86%	90.18%	0.056806
Living Room	MMLT	670	51.12%	45.07%	0.129880
	Ours	310	14.25%	78.35%	0.102854

Table 3. Table of statistics of equal-time comparison (2 hours for Breakfast, 1.5 hours for Villa, 1 hour for Bathroom, 25 minutes for Bidir, and 110 minutes for Living Room). Because of extra overheads for failure treatment in our method, the parameter of mutations per pixel should be set to a smaller value than in MMLT. We also show the comparisons of failure rate, acceptance rate and RMSE for these scenes. From the table, we can see that our method always produce better results (smaller RMSE) than MMLT does.

Breakfast Scene. Figure 1 shows an equal-time (2 hours) comparison on the Breakfast Scene which is illuminated by two lamps. Part of the scene, like the objects on the top of the desk, get direct illumination, however, the lighting for objects under the desk or over the lamps is much more complicated. From Figure 1 and Table 3, we can see that MMLT shows suboptimal performance because about

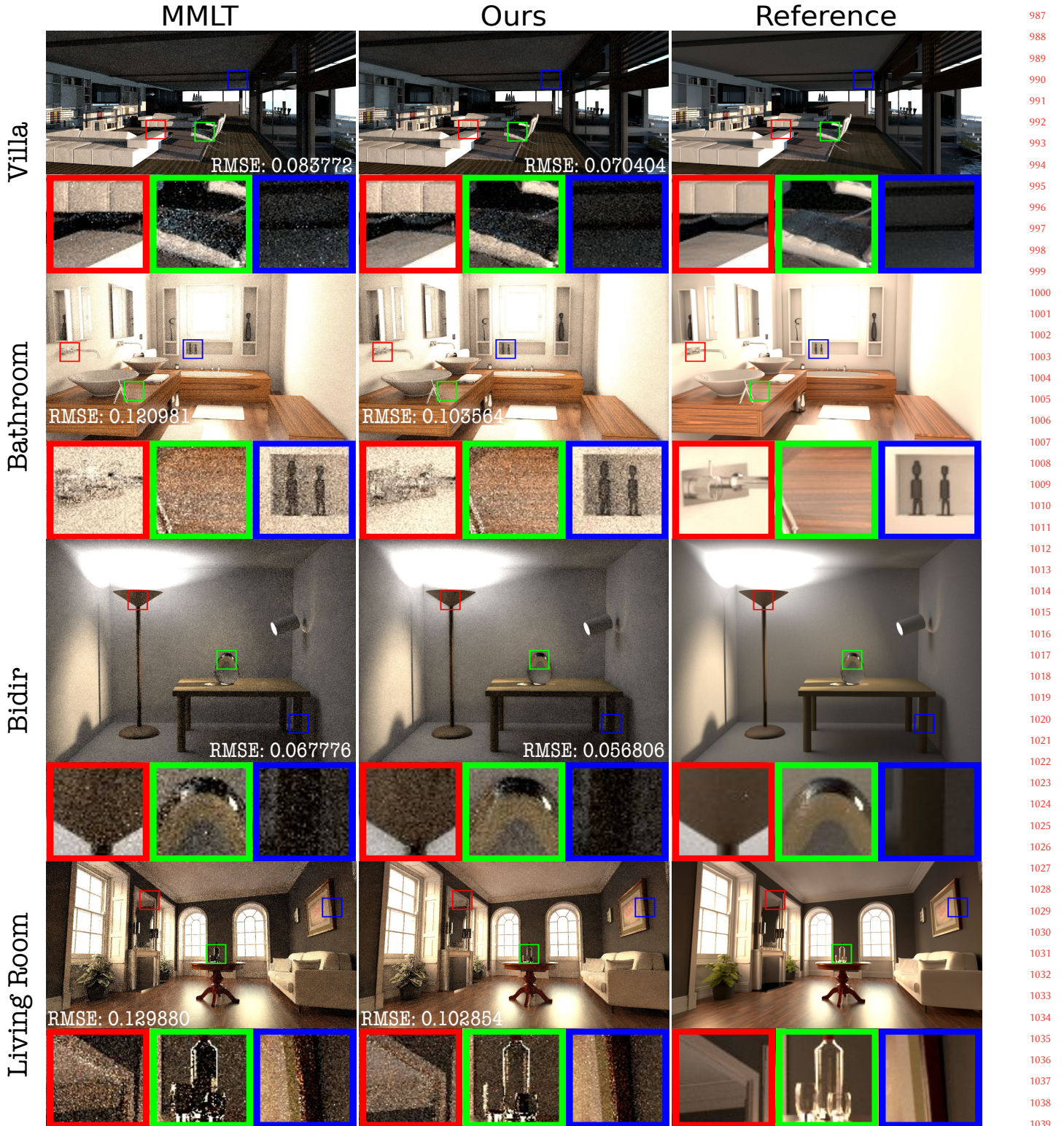


Fig. 3. *Equal-time comparisons*. These challenging scenes, Villa, Bathroom, Bidir and Living Room, are of various complex material, lighting and geometry. RMSE is used as the indicator of image quality. Our method always produce better results, with smaller RMSE, than MMLT does.

929
930
931
932
933
934
935
936
937
938
939
940
941
942
943
944
945
946
947
948
949
950
951
952
953
954
955
956
957
958
959
960
961
962
963
964
965
966
967
968
969
970
971
972
973
974
975
976
977
978
979
980
981
982
983
984
985
986
987
988
989
990
991
992
993
994
995
996
997
998
999
1000
1001
1002
1003
1004
1005
1006
1007
1008
1009
1010
1011
1012
1013
1014
1015
1016
1017
1018
1019
1020
1021
1022
1023
1024
1025
1026
1027
1028
1029
1030
1031
1032
1033
1034
1035
1036
1037
1038
1039
1040
1041
1042
1043
1044

37.37% of the paths that were used to reconstruct image carried no radiance. Giving special treatment to zero-contribution paths, our method reduces the percentage to around 1.54% and exhibits much better results with smaller RMSE. Our method distinguishes itself in those difficult settings where a large fraction of all of the possible proposal paths fail to carry any radiance in MMLT rendering, as shown in the three insets of Figure 1.

Villa Scene. The first part of Figure 3 shows an equal-time (1.5 hours) comparison on the Villa scene with complex materials and a difficult geometry configuration lit by outside environment daylight. This is a challenging scene because of the hard-to-find specular-diffuse-specular (SDS) light paths between the villa interior and the near-specular glass windows. The reference rendered by MMLT with 10000 mutations per pixel is still slightly noisy after several days of computation. Also, from Figure 3 and Table 3, we can see that MMLT produces a lot of noises because more than 62.81% of the paths that were used to reconstruct image were zero-contribution. Our method considers zero-contribution proposal as failure and gives special treatment to it. As a result, the percentage was reduced to about 14.47 and higher quality image was obtained. If our method is used to render the image with the same RMSE of 0.083772 like MMLT does, more than 37% of the time will be saved.

Bathroom Scene. The second part of Figure 3 shows an equal-time (1 hour) comparison on the Bathroom scene which contains several different materials including diffuse, specular, and glossy. The scene is illuminated with a large area light source directly visible from the camera. Unlike the Villa scene, the major part of the scene is directly illuminated by the light source. Even in such a simple lighting situation, our method can still produce a better image than MMLT does in equal time. If our method is used to render the image with the same RMSE of 0.120981 like MMLT does, more than 45% of the time will be saved.

Bidir Scene. The third part of Figure 3 shows an equal-time (25 minutes) comparison on the Bidir scene which is very classical. The illumination resembles the Breakfast scene whose part of objects get direct lighting and other parts not. If our method is used to render the image with the same RMSE of 0.067776 like MMLT does, about 28% of the time will be saved.

Living Room Scene. The last part of Figure 3 shows an equal-time (110 minutes) comparison on the Living Room scene. Light coming from outside environment enter the room through glass widows like the Villa scene does. Again, this kind of lighting makes rendering the scene a challenging task. What's more, the materials of the Living Room scene is more complex. The floor, the table and the paneling are made of substrate material, a layered model that varies between glossy specular and diffuse reflection depending on the viewing angle. The cups and the bottle on the table are glass. Other objects like the big mirror and the brushed stainless steel lampshades also contribute to the complication of materials of the scene. All of this result that more than 51.12% of all paths that were used to reconstruct image in MMLT don't carry any radiance. Again, our method is even more efficient in rendering scenes with complex material and lighting. If our method is used to render the image with the same RMSE of 0.129880 like MMLT does, about 47% of the time will be saved.

Convergence Comparison. To make our method more convincing, we did a sequence of comparisons with different computations and compared the convergence of MMLT and our method. We used ABCDEF and OPQRST to number the resulting images rendered by MMLT and our method respectively. The mutations per pixel of the images rendered with similar time were set as Table 4. The resulting comparison images were shown in Figure 4-(a).

MMLT	A	B	C	D	E	F
	20	40	85	170	340	670
Ours	O	P	Q	R	S	T
	10	20	35	75	150	310

Table 4. Table of parameter setting of mutations per pixel for convergence comparison.

Based on the comparison images and their error images in Figure 4-(a), we can see that our method converges much faster than MMLT does. To make this statement clearer, we calculated the RMSEs of each of these images and exhibited them in line chart as shown in Figure 4-(b).

As the blue dash lines mark in Figure 4-(b), the RMSE of image R rendered with our method is slightly smaller than the RMSE of image E rendered with MMLT, but the rendering time of image R is just about half of image E. Also, as the orange dash lines show the comparison the RMSE of image S and image F, our method saves even bigger ratio of time. So, we can deduce that: *the higher same-quality of images rendered by MMLT and our method, the bigger ratio of time will be saved by our method.*

6.2 Extra Results

In order to further verify the effectiveness of our method and the fact that other MLT-type algorithms can be easily extended with our method, we now do some comparison tests with RJMLT [Bitterli et al. 2018] with our method. We extend both RJMLT and MMLT in Bitterli's original source code, Tungsten [Bitterli 2017], a renderer that is a much simpler and faster than PBRT, and get two new algorithms, RJMLT+PF and MMLT+PF ("PF" means Proposal Failure). Considering that the random seeds used in RJMLT are not fixed, the result of any single run of RJMLT may not be representative, so average behavior of many times of rendering with exactly same settings is used to do comparison test with other algorithms, which is the very reason that we don't include RJMLT in all of tests of the prior scenes as shown in Figure 3.

Here, we'll compare equal-time images of the Glass-Of-Water scene rendered with the four algorithms in Tungsten, MMLT, RJMLT, MMLT+PF, RJMLT+PF. We set the maximum path length at 15 and *MaxRep* at 5, which is an empirical value. Expected results should be: MMLT+PF is better than MMLT, and RJMLT+PF is better than RJMLT. First, we produce the two five-minute images of MMLT and MMLT+PF. By the way, five-minute images are of relatively high quality because of the fact that Tungsten is much simpler and faster than PBRT. Second, we find the parameters of RJMLT and RJMLT+PF to produce five-minute images. Third, we run RJMLT and RJMLT+PF with the parameters 50 times to produce 50 images respectively. Fourth, calculate the average RMSEs of RJMLT and

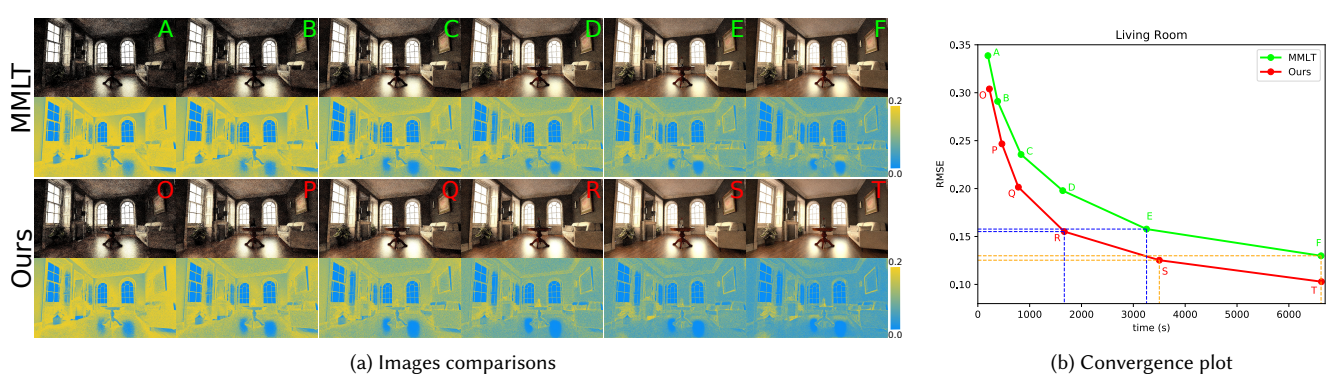


Fig. 4. *Convergence comparisons for the Living Room scene.* Based on the comparison images and their error images in (a), we can see that our method converges much faster than MMLT does. The RMSEs of each of these images are exhibited in line chart as (b). As the blue dash lines show, the RMSE of image R rendered with our method is slightly smaller than the RMSE of image E rendered with MMLT, but the rendering time of image R is just about half of image E. Also, as the orange dash lines show the comparison the RMSE of image S and image F, our method saves even bigger ratio of time.

RJMLT+PF with their own 50 images respectively. The Results are shown in Figure 5. For RJMLT and RJMLT+PF, while the two images are specially chosen from their own 50 images, which may not be representative, the RMSEs are the average of 50 results, which is reliable. In this scene, based on the RMSEs, we can see that: both RJMLT and MMLT+PF are better than MMLT; RJMLT+PF is the best (of course better than RJMLT); in particular, we get a bonus: *MMLT+PF is better than RJMLT*, which means that PF makes MMLT not just better than MMLT, but also better than RJMLT.

7 CONCLUSION

We first came up with the concept of *Proposal Failure*, and then presented a novel extension of MCMC, Proposal Failure MCMC (PFMCMC). A general example shown the effectiveness of PFMCMC. Furthermore, we applied PFMCMC to light transport simulation, getting a novel rendering algorithm, PFMLT. PFMLT is able to substantially decrease the rate of zero-contribution paths involved in reconstructing image and increases the overall efficiency a lot, which was verified by 5 challenging scenes. In order to further demonstrate that our algorithm is easy to implement and can be used to extend other MLT-type rendering algorithms, we extended MMLT and RJMLT in Tungsten renderer. With the test on the Glass-Of-Water scene, we exhibited that our method made RJMLT more efficient than the original RJMLT, and even made MMLT more efficient than the original RJMLT. All of these confirmed the general effectiveness of our method, the remedy for proposal failures.

7.1 Limitations and Future Work

During the extensions of our method to other algorithms, the corresponding parameters, like *MaxRep*, may need to be tuned correspondingly to reach optimal results. As a MLT-type rendering algorithm, generally, our method is also only good at rendering challenging scenes which contain complex materials and lighting. Like other adaptive MLT-type algorithms, such as *MEMLT* [Jakob and Marschner 2012], *H²MC* [Li et al. 2015], *HSLT* [Hanika et al. 2015] and *GeoMLT* [Otsu et al. 2018], extra computations are needed to

address challenging parts of scenes. So, the number of mutations per pixel that can be finished in equal time as non-adaptive algorithms decreases, which may slightly affect the rendering of simple parts of the same scene. Our method cannot change/improve the original nature of the MLT-type algorithm that is extended with our method. For example, RJMLT+PF inherited the nature that the random seeds used are not fixed from RJMLT, which means that the result of any single run of RJMLT+PF may also not be representative, so average behavior of many times of rendering with exactly same settings must be used to show its effectiveness.

Providing remedies to minimize the impact of proposal failure without modifying mutation strategies is a new direction to improve the efficiency of MLT-type algorithms. We just presented a simple remedy in this paper, and we believe that many more efficient and sophisticated remedies can be developed to further decrease the serious impact caused by proposal failures in the future research. Considering that MCMC is widely used in various fields, if necessary, the idea of remedy for proposal failures can be effectively introduced into these fields.

REFERENCES

- Benedikt Bitterli. 2017. Tungsten Source Code. (2017). <https://github.com/tunabrain/tungsten>.
- Benedikt Bitterli, Wenzel Jakob, Jan Novák, and Wojciech Jarosz. 2018. Reversible Jump Metropolis Light Transport using Inverse Mappings. *ACM Transactions on Graphics (Presented at SIGGRAPH)* 37, 1 (jan 2018). <https://doi.org/10.1145/3132704>
- S. Brooks, A. Gelman, G. L. Jones, and X. L. Meng. 2011. Handbook of Markov Chain Monte Carlo. *Chapman and Hall/CRC* (2011), 93–111.
- P. Giordani and R. Kohn. 2006. Adaptive independent Metropolis-Hastings by fast estimation of mixtures of normals. *Preprint* (2006).
- Adrien Gruson, Mickaël Ribardière, Martin Šík, Jiří Vorba, Rémi Cozot, Kadi Bouatouch, and Jaroslav Krivánek. 2017. A Spatial Target Function for Metropolis Photon Tracing. *ACM Trans. Graph.* 36, 1 (2017), 13. <https://doi.org/10.1145/2963097>
- H. Haario, E. Saksman, and J. Tamminen. 2001. An adaptive metropolis algorithm. *Bernoulli* 7 (2001), 223–242.
- Toshiya Hachisuka and Henrik Wann Jensen. 2011. Robust Adaptive Photon Tracing using Photon Path Visibility. *ACM Trans. Graph.* 30, 5 (2011). <https://doi.org/10.1145/2019627.2019633>
- Toshiya Hachisuka, Anton S. Kaplanyan, and Carsten Dachsbacher. 2014. Multiplexed Metropolis Light Transport. *ACM Trans. Graph. (Proceedings of SIGGRAPH)* 33, 4 (July 2014), 10. <https://doi.org/10.1145/2601097.2601138>

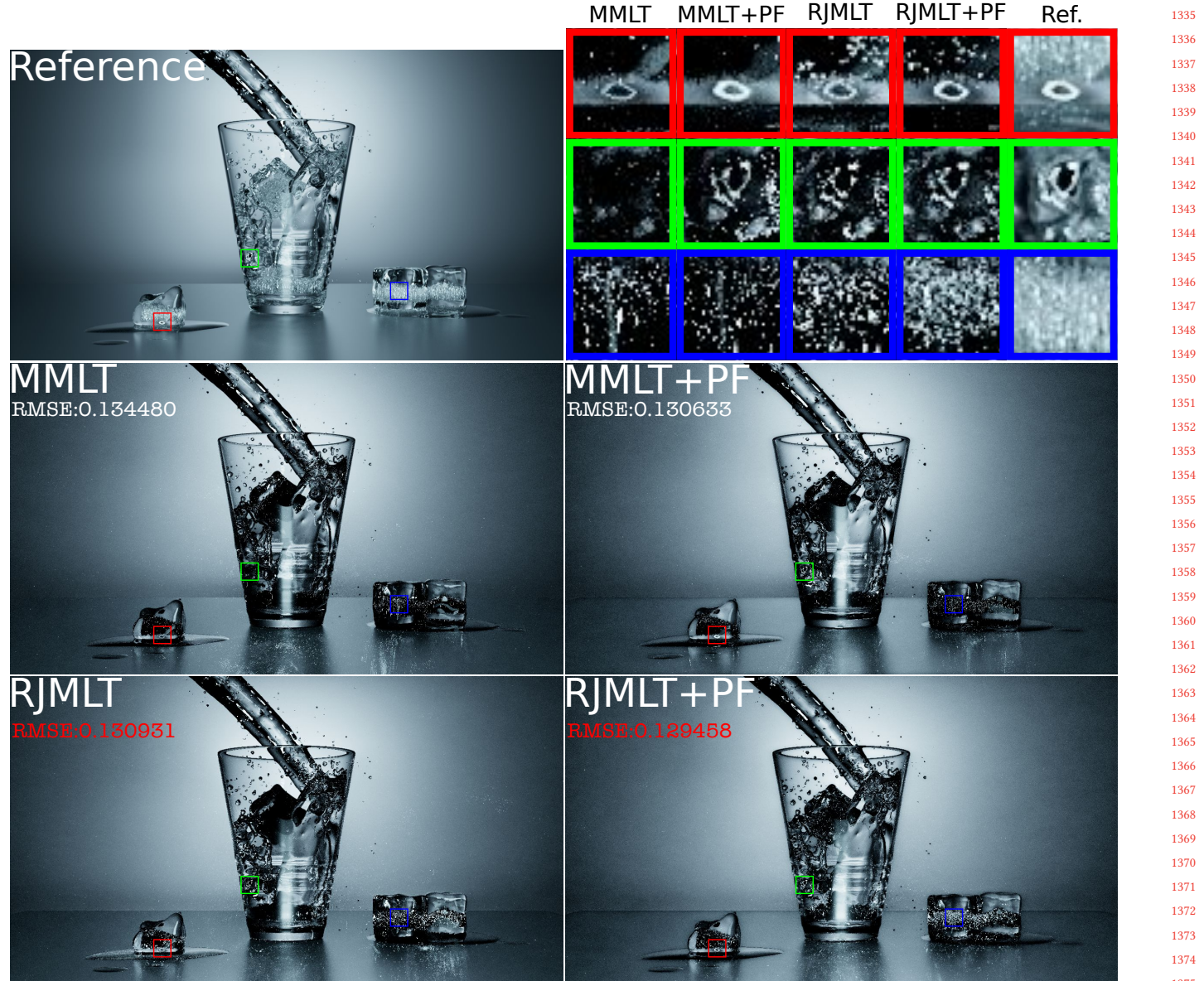


Fig. 5. *Equal-time comparisons with RJMLT.* "MMLT+PF" and "RJMLT+PF" are Proposal Failure extensions of MMLT and RJMLT respectively. Considering that the random seeds used in RJMLT are not fixed, the result of any single run of RJMLT may not be representative, so average behavior of many times of rendering with exactly same settings is used to do comparison test with other algorithms. For RJMLT and RJMLT+PF, while the two images are specially chosen from their own 50 images, which may not be representative, the RMSEs are the average of 50 results, which is reliable. In this scene, based on the RMSEs, we can see that: both RJMLT and MMLT+PF are better than MMLT; RJMLT+PF is the best (of course better than RJMLT); in particular, we get a bonus: *MMLT+PF is better than RJMLT*, which means that PF makes MMLT not just better than MMLT, but also better than RJMLT.

Johannes Hanika, Anton Kaplanyan, and Carsten Dachsbacher. 2015. Improved half vector space light transport. *Computer Graphics Forum (Proc. EGSR)* 34, 4 (2015), 65–74.
 W. K. Hastings. 1970. Monte Carlo sampling methods using Markov chains and their applications. *Biometrika* 57, 1 (1970), 97–109. <https://doi.org/10.1093/biomet/57.1.97>
 Jared Hoberock and John C. Hart. 2010. Arbitrary Importance Functions for Metropolis Light Transport. *Computer Graphics Forum* (2010), 1993–2003. <https://doi.org/10.1111/j.1467-8659.2010.01713.x>

Wenzel Jakob and Stephen Marschner. 2012. Manifold exploration: a Markov chain Monte Carlo technique for rendering scenes with difficult specular transport. *ACM Trans. Graph. (Proc. SIGGRAPH)* 31, 4 (2012).
 James T. Kajiya. 1986. The Rendering Equation. In *Computer Graphics (Proceedings of SIGGRAPH)* 20 (1986), 143–150. <https://doi.org/10.1145/15922.15902>
 C. Kelemen, L. Szirmay-Kalos, G. ANTAL, and F. CSONKA. 2002. A simple and robust mutation strategy for the Metropolis light transport algorithm. *Computer Graphics Forum* 21, 3 (July 2002), 531–540.

- 1393 Shinya Kitaoka, Yoshifumi Kitamura, and Fumio Kishino. 2009. Replica Exchange Light
1394 Transport. *Computer Graphics Forum* 28, 8 (2009), 2330–2342. <https://doi.org/10.1111/j.1467-8659.2009.01540.x> 1451
1395 Eric P. Lafortune and Yves D. Willems. 1993. Bi-Directional Path Tracing. *Proceedings*
1396 *of Compugraphics '93* (1993), 145–153. 1452
1397 Eric P. Lafortune and Yves D. Willems. 1996. Rendering Participating Media with Bidirectional
1398 Path Tracing. *Proceedings of the 7th Eurographics Workshop on Rendering* (1996), 91–100. 1453
1399 Tzu-Mao Li, Jaakkko Lehtinen, Ravi Ramamoorthi, Wenzel Jakob, and Frédéric Durand.
1400 2015. Anisotropic Gaussian Mutations for Metropolis Light Transport Through
1401 Hessian-Hamiltonian Dynamics. *ACM Trans. Graph. (Proc. SIGGRAPH Asia)* 34, 6
1402 (2015), 209:1–209:13. 1454
1403 N. Metropolis, N. Metropolis, M. N. Rosenbluth, A. H. Teller, and E. Teller. 1953. Equation
1404 of State Calculations by Fast Computing Machines. *J. Chem. Phys.* 21, 6 (1953), 1087–
1405 1092. <https://doi.org/10.1063/1.1699114> 1455
1406 Hisanari Otsu, Johannes Hanika, Toshiya Hachisuka, and Carsten Dachsbacher. 2018.
1407 Geometry-Aware Metropolis Light Transport. *ACM Transactions on Graphics (Proc.
1408 of SIGGRAPH Asia)* 37, 6, Article 278 (2018), 278:1–278:11 pages. 1456
1409 Hisanari Otsu, Anton S. Kaplanyan, Johannes Hanika, Carsten Dachsbacher, and
1410 Toshiya Hachisuka. 2017. Fusing State Spaces for Markov Chain Monte Carlo
1411 Rendering. *ACM Transactions on Graphics (Proc. of SIGGRAPH)* 36, 4, Article 74
1412 (2017), 74:1–74:10 pages. 1457
1413 Jacopo Pantaleoni. 2017. Charted Metropolis Light Transport. *ACM Transactions on
1414 Graphics* 36 (2017). 1458
1415 Gareth O. Roberts and Jeffrey S. Rosenthal. 2009. Examples of Adaptive MCMC. *Journal
1416 of Computational and Graphical Statistics* 18, 2 (2009), 349–367. <https://doi.org/10.1198/jcgs.2009.06134> 1459
1417 Benjamin Shaby and Martin T. Wells. 2010. Exploring an Adaptive Metropolis Algorithm.
1418 *Preprint* (2010). 1460
1419 E. Veach. 1997. Robust Monte Carlo Methods for Light Transport Simulation. *PhD
1420 thesis, Stanford University* (1997). 1461
1421 Eric Veach and Leonidas J. Guibas. 1994. Metropolis Light Transport. In *Photorealistic
1422 Rendering Techniques (Proceedings of the Eurographics Workshop on Rendering)* (1994),
1423 147–162. https://doi.org/10.1007/978-3-642-87825-1_11 1462
1424 Eric Veach and Leonidas J. Guibas. 1997. Metropolis Light Transport. In *Annual
1425 Conference Series on Computer Graphics (Proceedings of SIGGRAPH)* (1997), 65–76.
1426 https://doi.org/10.1145/258734.258775 1463
1427 Matti Vihola. 2012. Robust Adaptive Metropolis Algorithm with Coerced Acceptance
1428 Rate. *Statistics and Computing* 22, 5 (2012), 997–1008. 1464
1429 Martin Šík, Hisanari Otsu, Toshiya Hachisuka, and Jaroslav Krivánek. 2016. Robust Light
1430 Transport Simulation via Metropolised Bidirectional Estimators. *ACM Transactions
1431 on Graphics (Proceedings of SIGGRAPH Asia)* 35, 6 (Nov. 2016), 12. <https://doi.org/10.1145/2980179.2982411> 1465
1432
1433
1434
1435
1436
1437
1438
1439
1440
1441
1442
1443
1444
1445
1446
1447
1448
1449
1450

A THE IMPORTANCE OF "J --"

Line 29 in Algorithm 2, " $j--$ ", is very important, because j is used to draw proposal vector of random numbers \bar{v} from \bar{u} in primary sample space. " $j--$ " is the very operation that prevents the new proposal " \bar{v} " from the impact of the current proposal failure. As shown in Figure 4, Image D and Image R are equal-time rendering results of MMLT and PFMLT(without " $j--$ ") respectively, and as shown in Table 4, the mutations per pixel for Image D and Image R are 170 and 75 respectively. In order to show the importance of " $j--$ ", we need to produce another rendering result D-R with PFMLT(without " $j--$ ") with the mutations per pixel as 170.

As shown in Figure 6, the fact that the quality of Image D-R is much lower than Image R shows the importance of " $j--$ " operation. Why is Image D-R worse than Image D? Considering that, for proposal failure path, MMLT uses the contribution of the current path, while PFMLT(without " $j--$ ") uses zero-contribution, it is of uncertainty that which one of the two kinds of contribution is more proximately proportional to the probability with which the proposal failure was sampled. So, whether PFMLT(without " $j--$ ") produces a better or worse result than MMLT does is normal.

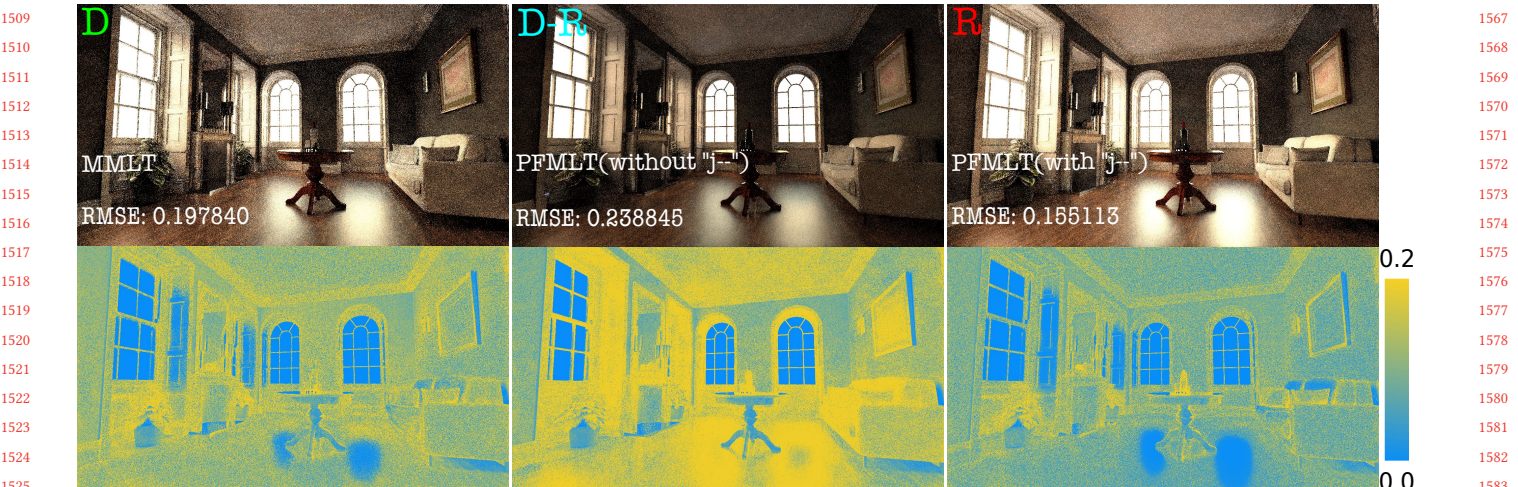


Fig. 6. *Equal-time "j --" comparisons.* Image D, Image D-R, Image R are rendered with MMLT, PFMLT(without "j --") and PFMLT(with "j --") respectively. The fact that the quality of Image D-R is much lower than Image R shows the importance of "j --" operation. Why is Image D-R worse than Image D? Considering that, for proposal failure path, MMLT uses the contribution of the current path, while PFMLT(without "j --") uses zero-contribution, it is of uncertainty that which one of the two kinds of contribution is more proximately proportional to the probability with which the proposal failure was sampled. So, whether PFMLT(without "j --") produces a better or worse result than MMLT does is normal.

1509
1510
1511
1512
1513
1514
1515
1516
1517
1518
1519
1520
1521
1522
1523
1524
1525
1526
1527
1528
1529
1530
1531
1532
1533
1534
1535
1536
1537
1538
1539
1540
1541
1542
1543
1544
1545
1546
1547
1548
1549
1550
1551
1552
1553
1554
1555
1556
1557
1558
1559
1560
1561
1562
1563
1564
1565
1566

1567
1568
1569
1570
1571
1572
1573
1574
1575
1576
1577
1578
1579
1580
1581
1582
1583
1584
1585
1586
1587
1588
1589
1590
1591
1592
1593
1594
1595
1596
1597
1598
1599
1600
1601
1602
1603
1604
1605
1606
1607
1608
1609
1610
1611
1612
1613
1614
1615
1616
1617
1618
1619
1620
1621
1622
1623
1624